Supplementary Information

Plasmonic Coupling of Silver Nanospheres Loaded on Cobalt-Iron Layered Double Hydroxides: A Robust SERS Probe for 4-Nitrophenol Detection

Thangavelu Kokulnathan[a], Kalingarayanpalayam Matheswaran Arun Kumar[a], Tzyy-Jiann Wang[a*], Elumalai Ashok Kumar[a], Allen Joseph Anthuvan[a,b], Kai-Jiun Chen[a], Yung-Yu Liang[a]

[a] *Department of Electro-Optical Engineering, National Taipei University of Technology, Taipei 10608, Taiwan.*

[b] *Nanotech Division, Accubits Invent Pvt. Ltd, Trivandrum 695 592, Kerala, India.*

***Corresponding Author**

E-mail: f10939@ntut.edu.tw

Materials and reagents

Silver nitrate ($AgNO_3$), polyvinylpyrrolidone (PVP, average molecular weight ~ 40,000), hydrazine monohydrate ($N_2H_2 \cdot H_2O$), cobalt(II) nitrate hexahydrate ($Co(NO_3)_2 \cdot 6H_2O$), ferric nitrate nonahydrate ($Fe(NO_3)_3 \cdot 9H_2O$), urea (CH_4N_2O), and 4-NP were purchased from Sigma-Aldrich. All of the chemicals in this research were analytical grade and used without further purification. Deionized (DI) water was used throughout all aqueous solutions.

Instrumentation

The crystal structures of the synthesized materials were analyzed by X-Ray Diffractometer (XRD, PANalytical). The chemical valence states of the elements in the synthesized materials were examined by an X-ray photoelectron spectrometer (XPS, JEOL JPS-9030). The material morphology was observed by the field-emission scanning electron microscope (FE-SEM, JEOL 6500F and JEOL JSM-7800F Prime) equipped with the energy dispersive spectrometer (EDS) and elemental mapping apparatus. SERS spectra were measured by using the 532 nm diode pumped solid state laser and the optical spectrometer (Princeton instrument, Acton SP-2358) equipped with the TE-cooled CCD (Princeton instrument, PIXIS 100). All Raman spectra were measured using a 100× objective lens with an integration time of 10 sec.

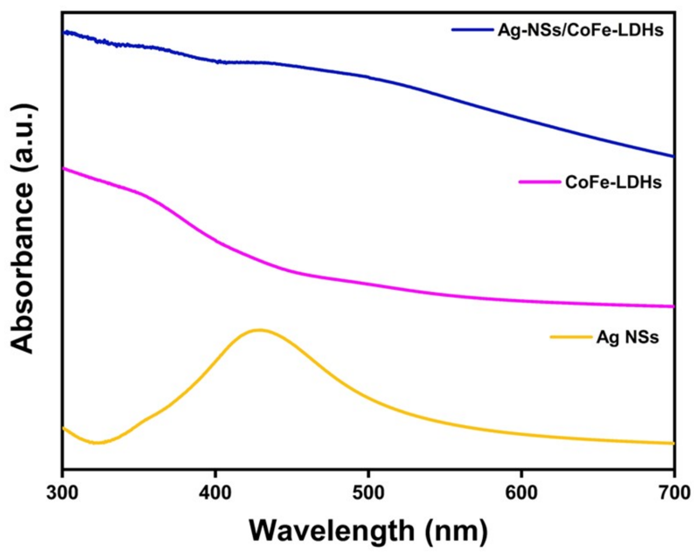

Fig. S1 UV-Vis spectra of Ag NSs, CoFe-LDHs, and Ag-NSs/CoFe-LDHs nanocomposite.

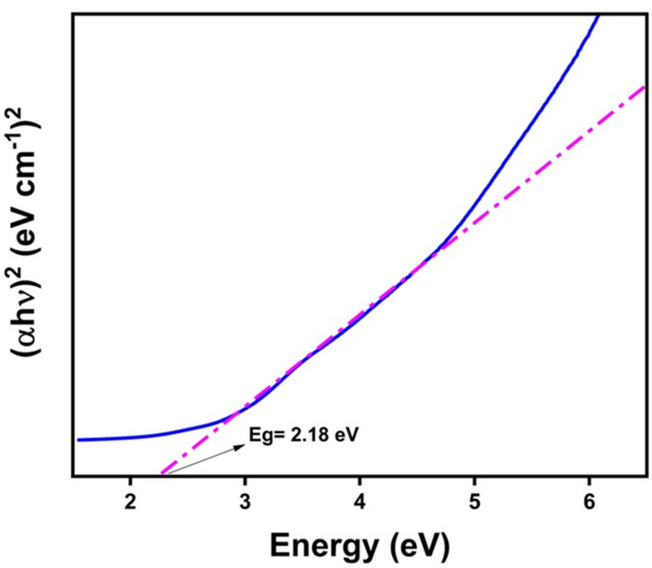

Fig. S2 Tauc plot for CoFe-LDHs.

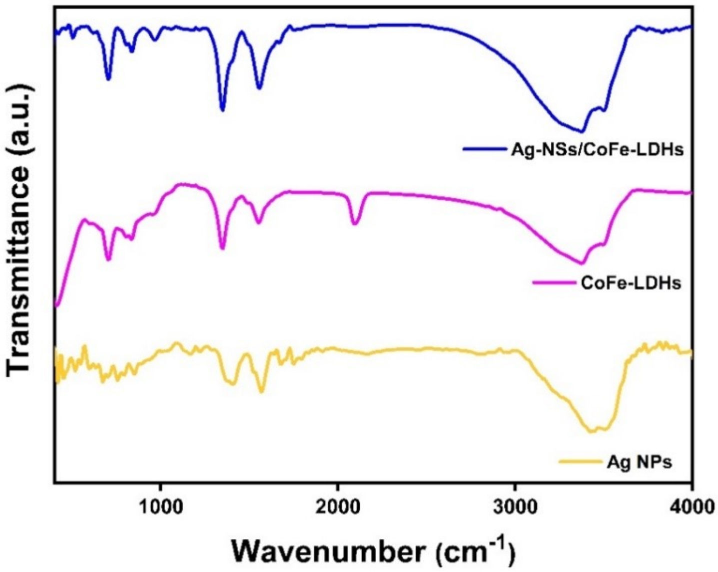

Fig. S3 FT-IR spectra of Ag NSs, CoFe-LDHs, and Ag-NSs/CoFe-LDHs nanocomposite.

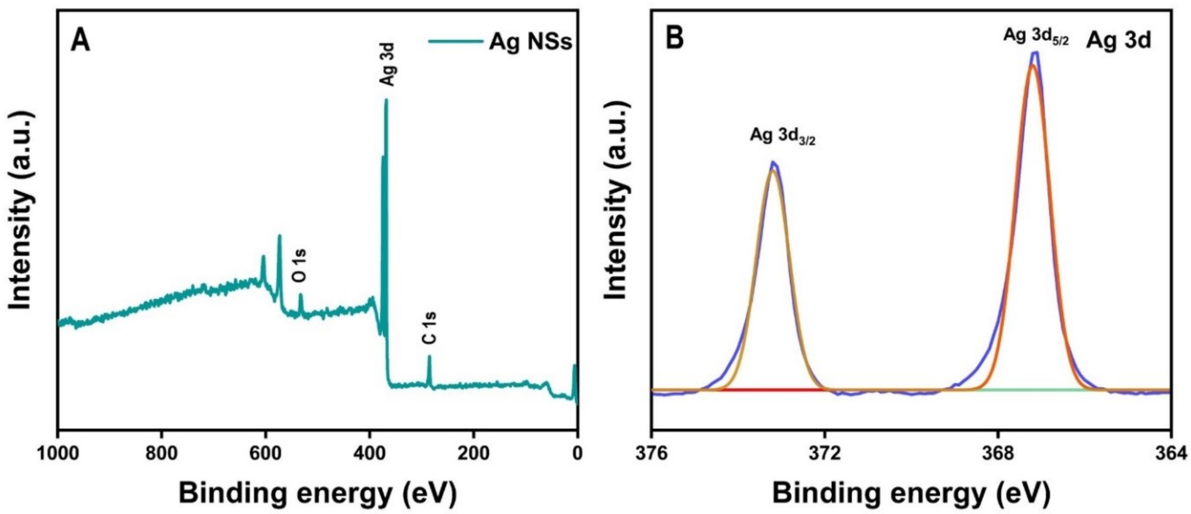

Fig. S4 (A) XPS survey spectrum and (B) high-resolution XPS spectrum for Ag 3d of Ag NSs.

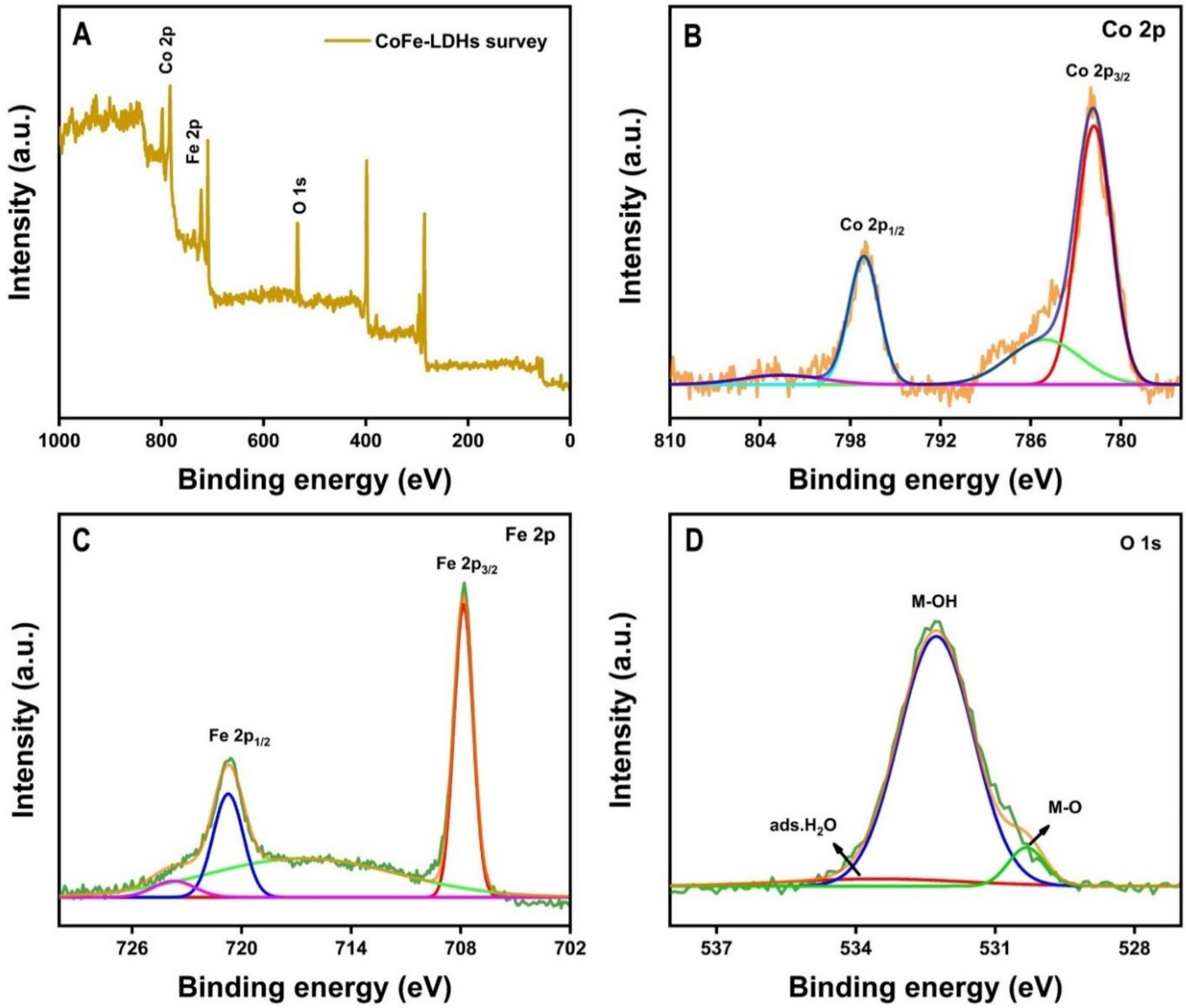

Fig. S5 (A) XPS survey spectrum of CoFe-LDHs. High-resolution XPS spectra for (B) Co 2p, (C) Fe 2p, and (D) O 1s of CoFe-LDHs

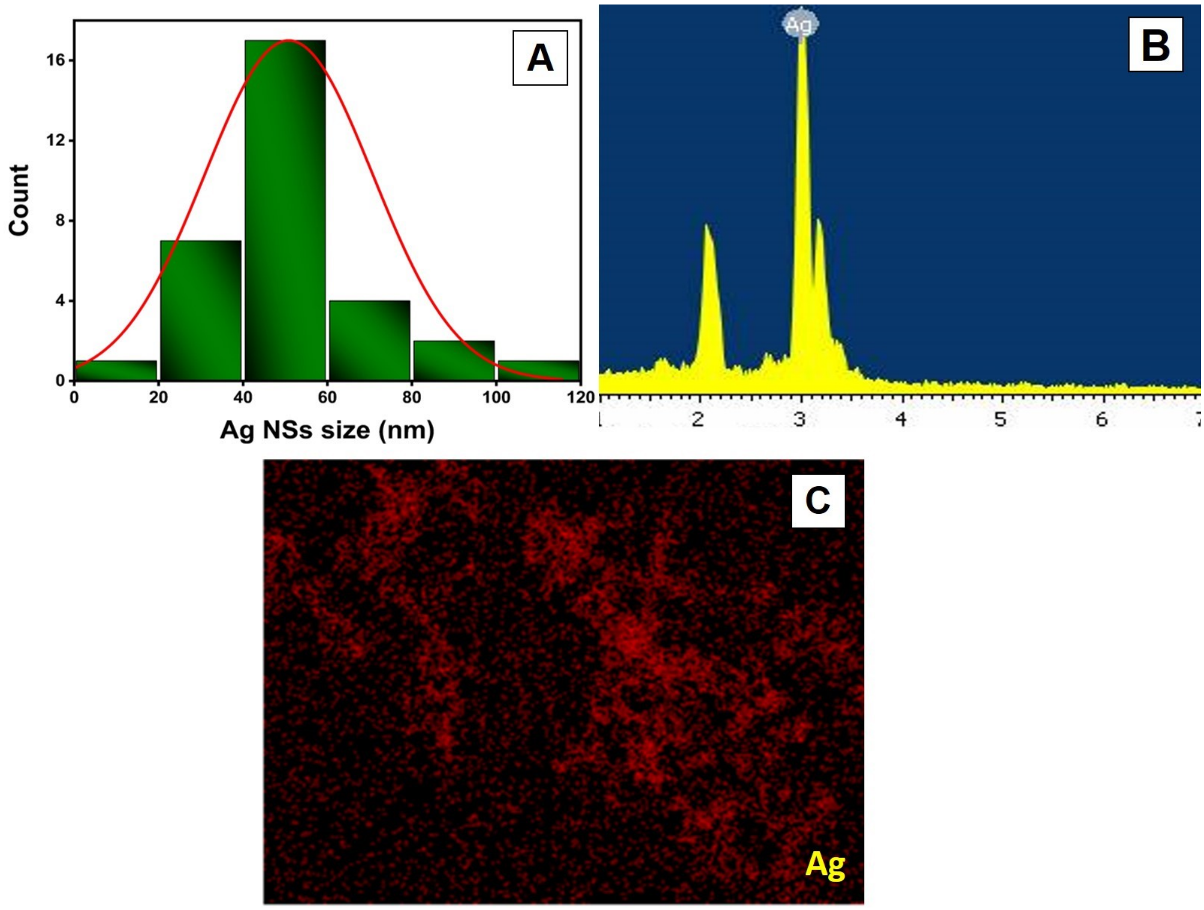

Fig. S6 (A) Histogram of particle size distribution, (B) EDX spectrum, and (C) elemental mapping image of Ag NSs.

.

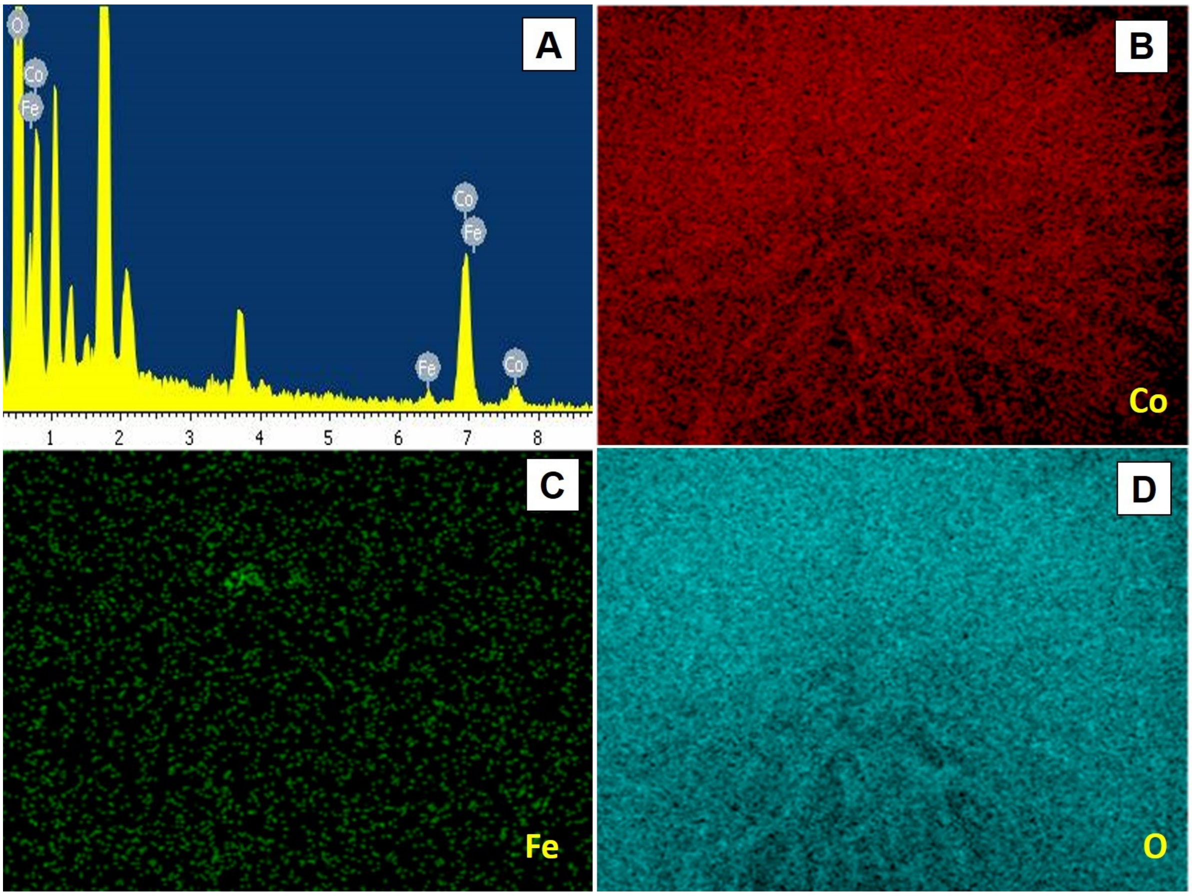

Fig. S7 (A) EDX analysis and (B–D) elemental mapping of CoFe-LDHs.

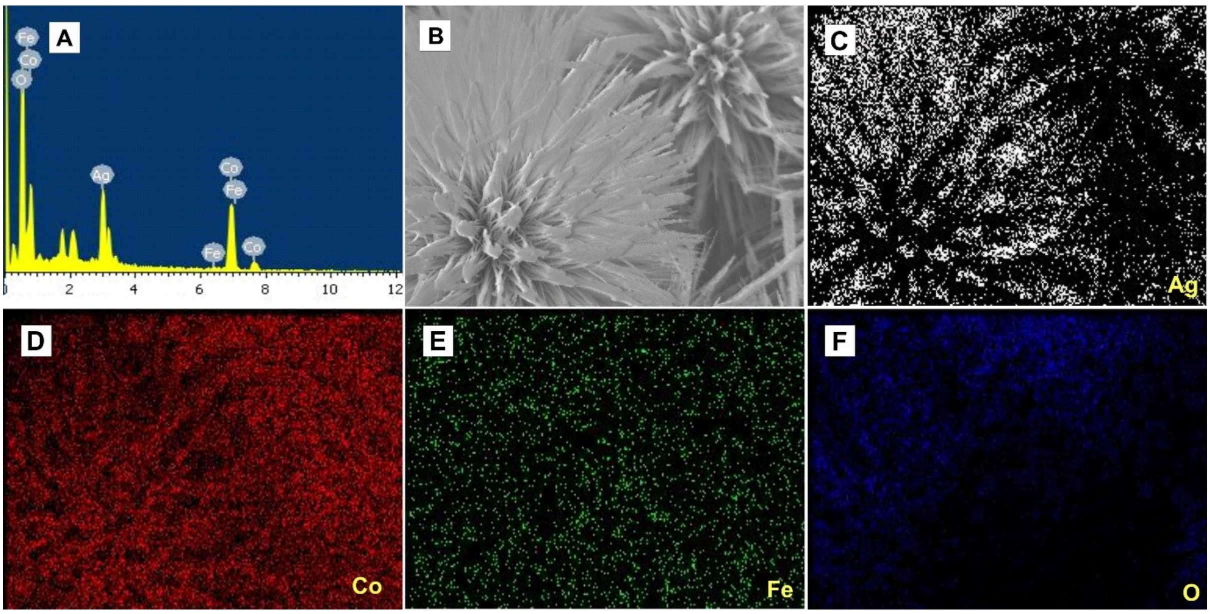

Fig. S8 (A) EDX spectrum and (B) FESEM image of the Ag-NSs/CoFe-LDHs nanocomposite, (C–F) corresponding elemental mapping images for Ag, Co, Fe, and O elements

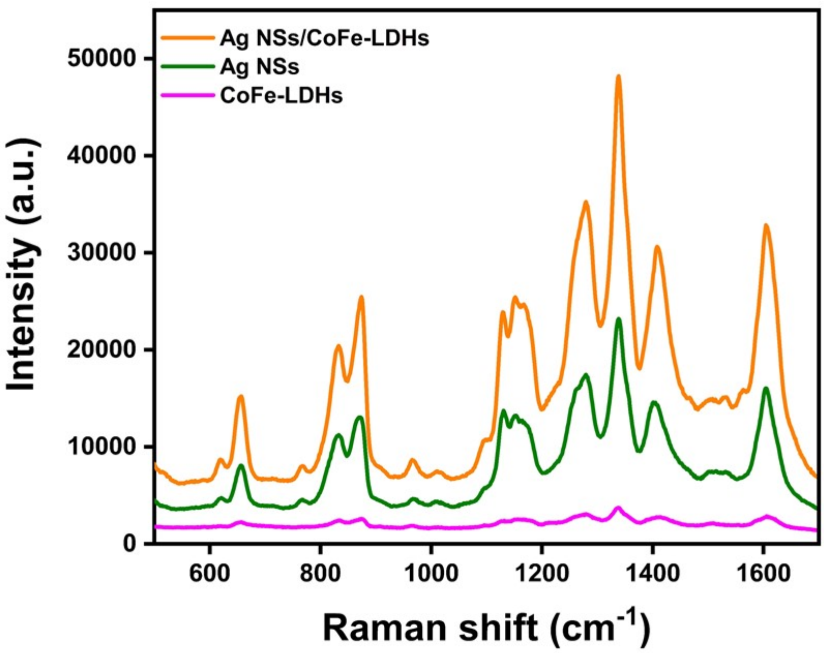

Fig. S9 SERS response of 4-NP with the concentration of 10^{-4} M on the CoFe-LDHs, the Ag NSs, and the Ag-NSs/CoFe-LDHs nanocomposite.

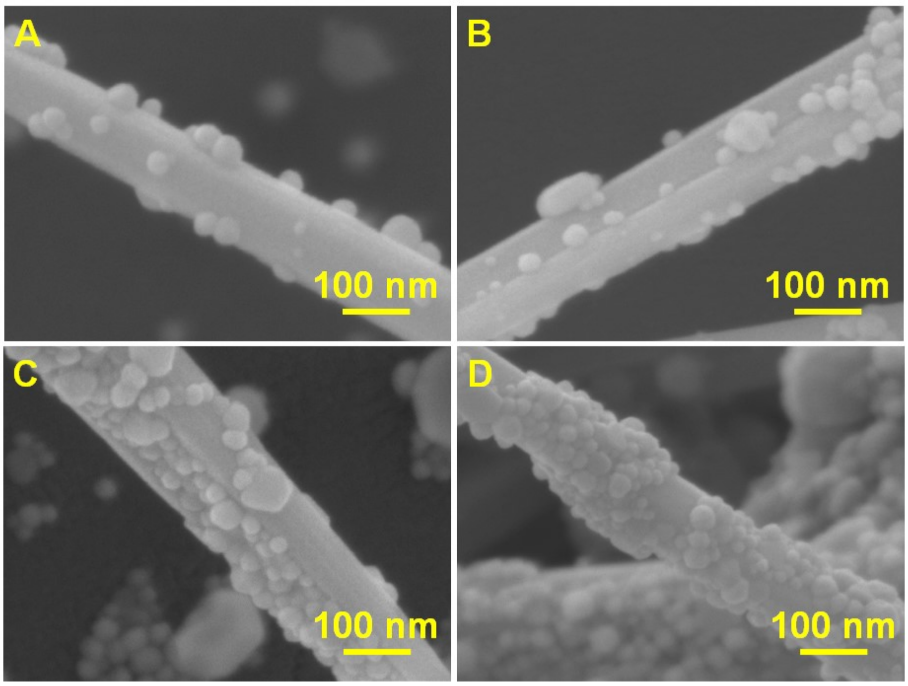

Fig. S10 FESEM images of Ag-NSs/CoFe-LDHs nanocomposite prepared with the volumes of Ag NSs solution (A) 200 µL, (B) 300 µL, (C) 400 µL, and (D) 500 µL.

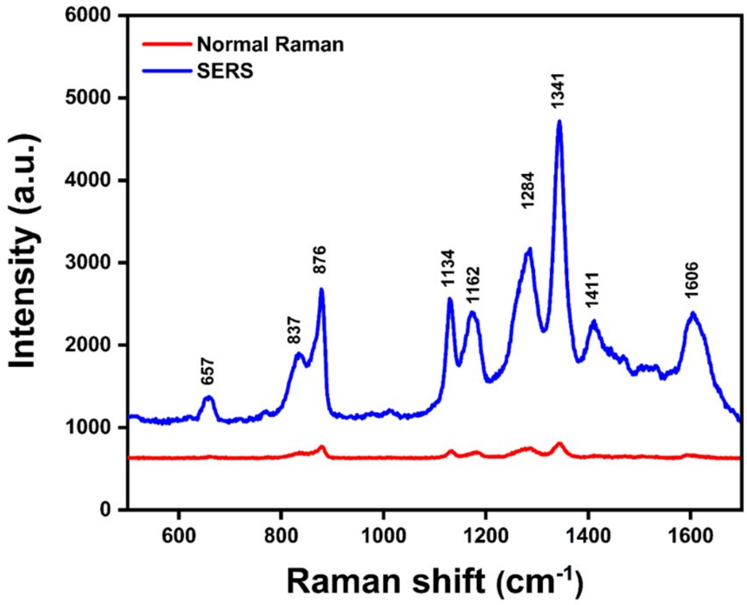

Fig. S11 Comparison of normal Raman and SERS spectra of 4-NP on the glass substrate (10^{-2} M) and the Ag NSs/CoFe-LDHs SERS substrate (10^{-13} M).

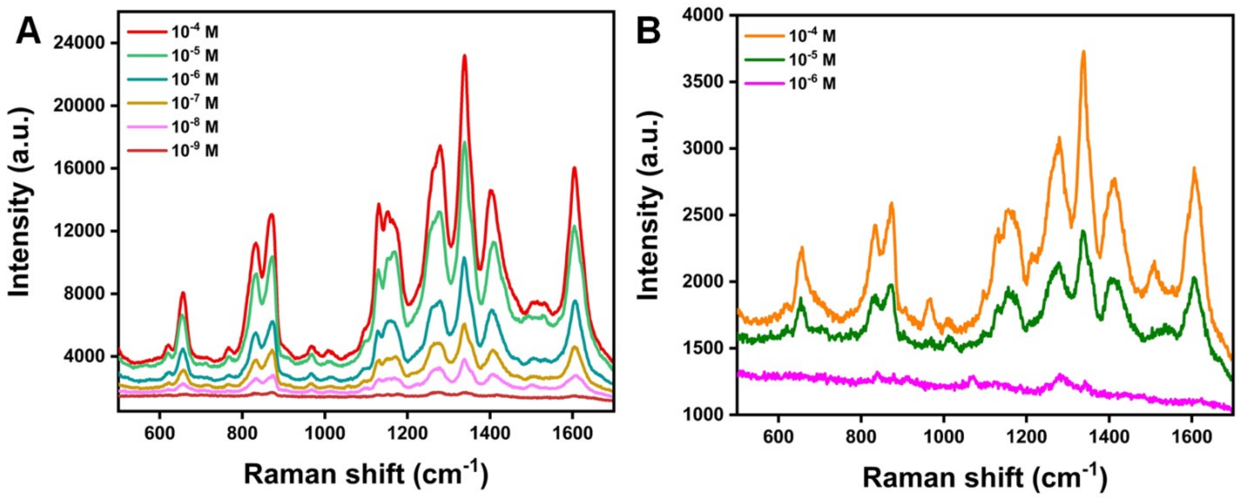

Fig. S12 SERS spectra of 4-NP with different concentrations on (A) the Ag NSs (10^{-4}–10^{-9} M) and (B) the CoFe-LDHs (10^{-4}–10^{-6} M).

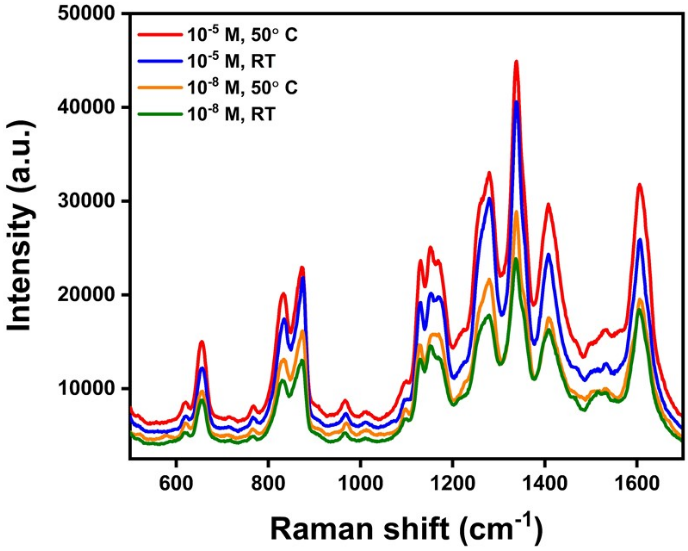

Fig. S13 Comparison of SERS spectra of 4-NP on the Ag-NSs/CoFe-LDHs SERS substrates dried at 20 ºC (room temperature, RT) and 50 ºC.

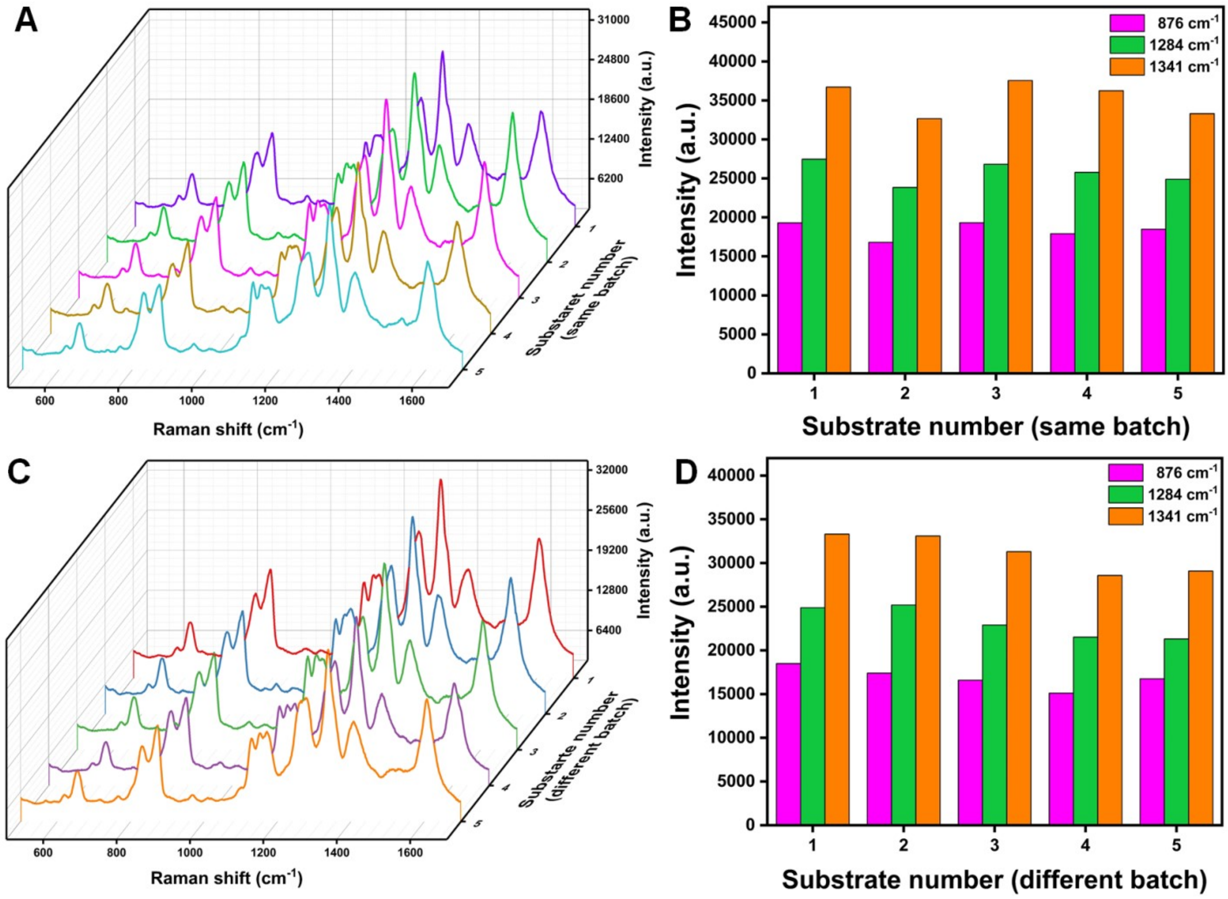

Fig. S14 Reproducibility test of the Ag-NSs/CoFe-LDHs SERS substrates prepared within **(A)** the same batch and **(C)** different batches for the detection of 4-NP (10^{-7} M). Distribution of Raman peak intensities at 876, 1284 and 1341 cm^{-1} for the reproducibility test within **(B)** the same batch and **(D)** different batches.

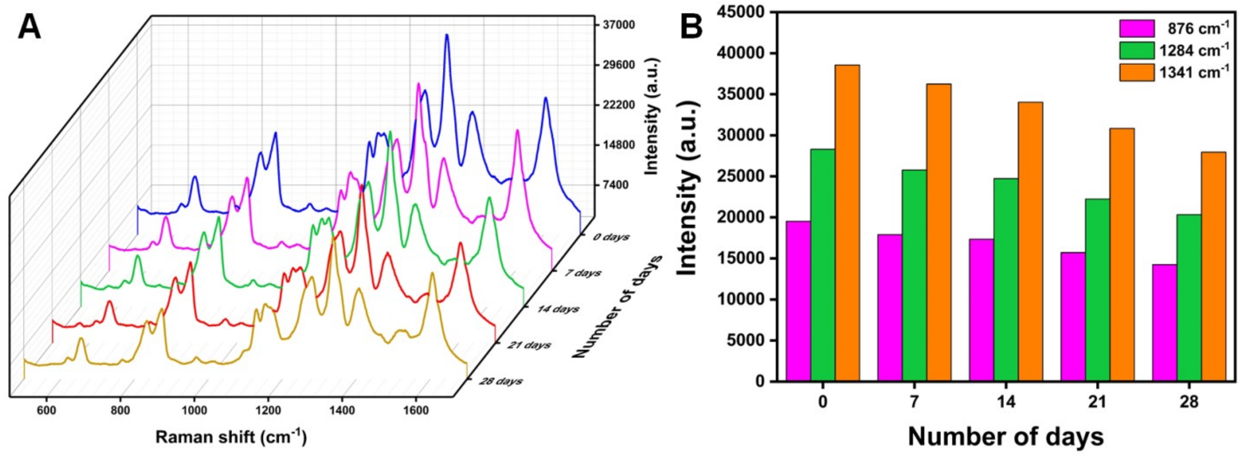

Fig. S15 (A) SERS spectra of 4-NP (10^{-7} M) on the Ag-NSs/CoFe-LDHs measured at the 7-day interval over the duration of 28 days. (B) Corresponding normalized Raman peak intensities of 4-NP as a function of the number of storage days.

Table S1 Raman band assignment of 4-NP **[S1]**

Raman shift (cm^{-1})	**Band assignment**
657	C=O out-of-plane bending
837	C-H out-of-plane bending
876	NO_2 bending
1134	C-H in-plane bending
1162	C-H in-plane bending
1284	ring deformation mixed with NO_2 group
1341	symmetric stretching mode of NO_2 group
1411	C-H in-plane bending
1606	ring stretching

Table S2 Performance comparison of various SERS-active materials for 4-NP detection.

Material	**Preparation method**	**LOD (M)**	**EF**	**Ref.**
Ag/ZnO[1]	chemical reduction and co-precipitation	1.49×10^{-13}	4.27×10^{10}	S1
ZnO NW/Ag NPs[2]	sonication, annealing	1×10^{-4}	-	S2
ER-Au[3]	electrochemical roughening	10^{-9}	-	S3
Au NCs[4]	seed-mediated growth	4.3×10^{-6}	1.9×10^{8}	S4
Ag/PDMS[5]	curing	5.7×10^{-7}	-	S5
Ag-NSs/CoFe-LDH	hydrothermal method and chemical reduction	2.36×10^{-14}	5.65×10^{11}	**this work**

[1] ZnO multipods decorated with Ag nanospheres

[2] silver nanoparticles decorated on ZnO nanowires

[3] electrochemically roughened nano-Au

[4] gold nanocubes

[5] polydimethylsiloxane with embedded Ag nanoparticles

Table S3 Performance comparison of various detection methods for 4-NP detection.

Material	Preparation method	Detection method	LOD (M)	Ref
Cu, N–CDs[1]	hydrothermal method	chemiluminescence	6×10^{-11}	S6
Fe_3O_4/Ag-FM[2]	hydrothermal method	ECD[8]	9.3×10^{-8}	S7
PDPP–GO[3]	Hummers' method	ECD[8]	1×10^{-7}	S8
NiO/SPCE[4]	phytochemical synthesis	ECD[8]	5.19×10^{-10}	S9
NiO/CeO_2[5]	ignition method	ECD[8]	2.48×10^{-6}	S10
MIP@CQDs[6]	sol-gel imprinting process	FL[9]	4×10^{-7}	S11
BSA Au-NCs Test paper[7]	BSA assisted reduction	FL[9]	1×10^{-9}	S12
Ag-NSs/ CoFe-LDH	hydrothermal method and chemical reduction	SERS	2.36×10^{-14}	**this work**

[1] copper and nitrogen co-doped carbon dots (CD)

[2] Ag-incorporated 3D flower-like porous Fe_3O_4 magnetic microstructure

[3] pyridine diketopyrrolopyrrole (PDPP)-functionalized graphene oxide

[4] NiO nanoparticles onto the screen-printed carbon electrode

[5] nickel oxide/cerium oxide

[6] molecularly imprinted polymers (MIP) coating on the carbon dots

[7] bovine serum albumin (BSA) functionalized fluorescent gold nanocluster

[8] electro chemical detection

[9] fluorescence

Table S4 Detection of 4-NP in the river water by the Ag-NSs/CoFe-LDHs SERS substrate.

Raman peak	Spiked concentration	Measured concentration	Recovery rate
876 cm^{-1}	1×10^{-5} M	9.2×10^{-4} M	92.51 %
	1×10^{-8} M	9.5×10^{-7} M	95.32 %
	1×10^{-11} M	9.1×10^{-10} M	91.25 %
1284 cm^{-1}	1×10^{-5} M	9.5×10^{-4} M	95.32 %
	1×10^{-8} M	9.3×10^{-7} M	93.07 %
	1×10^{-11} M	7.7×10^{-10} M	77.90 %
1341 cm^{-1}	1×10^{-5} M	9.5×10^{-4} M	96.02 %
	1×10^{-8} M	9.4×10^{-7} M	94.84 %
	1×10^{-11} M	9.3×10^{-10} M	81.93 %

References

S1. Kumar, E. A.; Barveen, N. R.; Wang, T.-J.; Kokulnathan, T.; Chang, Y.-H. Development of SERS platform based on ZnO multipods decorated with Ag nanospheres for detection of 4-nitrophenol and rhodamine 6G in real samples. *Microchemical Journal* **2021**, *170*, 106660.

S2. Fularz, A.; Almohammed, S.; Rice, J. H. Oxygen incorporation-induced SERS enhancement in silver nanoparticle-decorated ZnO nanowires. *ACS Applied Nano Materials* **2020**, *3* (2), 1666-1673.

S3. Wang, J.; Qiu, C.; Mu, X.; Pang, H.; Chen, X.; Liu, D. Ultrasensitive SERS detection of rhodamine 6G and p-nitrophenol based on electrochemically roughened nano-Au film. *Talanta* **2020**, *210*, 120631.

S4. Parambath, J. B.; Kim, G.; Han, C.; Mohamed, A. A. SERS performance of cubic-shaped gold nanoparticles for environmental monitoring. *Research on Chemical Intermediates* **2023**, *49* (3), 1259-1271.

S5. Wang, M.; De Vivo, B.; Lu, W.; Muniz-Miranda, M. Sensitive surface-enhanced Raman scattering (SERS) detection of nitroaromatic pollutants in water. *Applied spectroscopy* **2014**, *68* (7), 784-788.

S6. Delnavaz, E.; Amjadi, M. An ultrasensitive chemiluminescence assay for 4-nitrophenol by using luminol–$NaIO_4$ reaction catalyzed by copper, nitrogen co-doped carbon dots. *Spectrochimica Acta Part A: Molecular and Biomolecular Spectroscopy* **2020**, *241*, 118608.

S7. Vo, T. K.; Nguyen, T. H. A.; Dinh, Q. K.; Nguyen, V. C. Dual role of flower-like Fe_3O_4/Ag microstructure in electrocatalytic detection and catalytic reduction of 4-nitrophenol. *Materials Science in Semiconductor Processing* **2023**, *160*, 107441.

S8. Jia, L.; Hao, J.; Wang, S.; Yang, L.; Liu, K. Sensitive detection of 4-nitrophenol based on pyridine diketopyrrolopyrrole-functionalized graphene oxide direct electrochemical sensor. *RSC Advances* **2023**, *13* (4), 2392-2401.

S9. Somasundaram, G.; Balasubramanian, S.; Vaiyapuri, T.; Muthiah, S.; Sivanesan, J. R.; Nesakumar, N.; Shanmugam, S.; Gunasekaran, B. M. Electrochemical detection of 4-nitrophenol using a screen-printed carbon electrode modified by rod-shaped nickel oxide nanoparticles. *ChemistrySelect* **2023**, *8* (9), e202204418.

S10. Ahmad, N.; Alam, M.; Wahab, R.; Ahmad, J.; Ubaidullah, M.; Ansari, A. A.; Alotaibi, N. M. Synthesis of NiO–CeO_2 nanocomposite for electrochemical sensing of perilous 4-nitrophenol. *Journal of Materials Science: Materials in Electronics* **2019**, *30*, 17643-17653.

S11. Wang, K.; Tan, L.; Zhang, Y.; Zhang, D.; Wang, N.; Wang, J. A molecular imprinted fluorescence sensor based on carbon quantum dots for selective detection of 4-nitrophenol in aqueous environments. *Marine Pollution Bulletin* **2023**, *187*, 114587.
S12. Yang, X.; Wang, J.; Su, D.; Xia, Q.; Chai, F.; Wang, C.; Qu, F. Fluorescent detection of TNT and 4-nitrophenol by BSA Au nanoclusters. *Dalton transactions* **2014**, *43* (26), 10057-10063.